LAWRENCE
LIVERMORE
NATIONAL
LABORATORY

LLNL-CONF-614133

Thick Diffusion Limit Boundary Layer Test Problems

T. S. Bailey, J. H. Chang, J. S. Warsa, M. L. Adams

January 30, 2013

International Conference on Mathematics and Computational Methods Applied to Nuclear Science and Engineering
Sun Valley, ID, United States
May 5, 2013 through May 9, 2013

Disclaimer

International Conference on Mathematics and Computational Methods Applied to Nuclear Science & Engineering (M&C 2013), Sun Valley, Idaho, USA, May 5-9, 2013, on CD-ROM, American Nuclear Society, LaGrange Park, IL (2013)

THICK DIFFUSION LIMIT BOUNDARY LAYER TEST PROBLEMS

Teresa S. Bailey
Lawrence Livermore National Laboratory
7000 East Avenue, L-095
Livermore, CA 94551
bailey42@llnl.gov

Jae H. Chang and James S. Warsa
Los Alamos National Laboratory
P.O. Box 1663, MS D409
Los Alamos, NM 87544
jhchang@lanl.gov; warsa@lanl.gov

Marvin L. Adams
Texas A&M University
Department of Nuclear Engineering
College Station, TX 77843-3133
mladams@tamu.edu

ABSTRACT

We develop two simple test problems which quantify the behavior of computational transport solutions in the presence of boundary layers that are not resolved by the spatial grid. In particular we study the quantitative effects of "contamination" terms that, according to previous asymptotic analyses, may have a detrimental effect on the solutions obtained by both discontinuous finite element (DFEM) and characteristic-method (CM) spatial discretizations, at least for boundary layers caused by azimuthally asymmetric incident intensities. Few numerical results have illustrated the effects of this contamination, and none have quantified it to our knowledge. Our test problems use leading-order analytic solutions that should be equal to zero in the problem interior, which means the observed interior solution is the error introduced by the contamination terms. Results from DFEM solutions demonstrate that the contamination terms can cause error propagation into the problem interior for both orthogonal and non-orthogonal grids, and that this error is much worse for non-orthogonal grids. This behavior is consistent with the predictions of previous analyses. We conclude that these boundary layer test problems and their variants are useful tools for the study of errors that are introduced by unresolved boundary layers in diffusive transport problems.

Key Words: Asymptotic Diffusion Limit Analysis, Deterministic Transport, Boundary Layer, Finite Element Methods, Characteristic Methods

1. INTRODUCTION

Diffusion-limit asymptotic analysis has been a powerful tool for understanding the suitability of discretizations for the linear Boltzmann transport equation when applied to thick, diffusive problems. Much analysis and many test problems have demonstrated that Discontinuous Finite

Element Methods (DFEM) with properly chosen weight and basis functions and Characteristic Methods (CM) with properly chosen spatial moments and source approximations will produce leading-order solutions that satisfy reasonable diffusion discretizations in the interior of diffusive problems, which is the desired behavior. However, the analysis also shows that the boundary conditions satisfied by these leading-order solutions may be inaccurate if the spatial grid does not resolve boundary layers. For standard, upwind DFEMs and CMs, the effective boundary condition can be written in terms of two components. The first component is a good approximation of the boundary condition satisfied by the analytic (exact) leading-order solution. The second component is a "contamination" term that is zero if the incident intensity is azimuthally symmetric about the local normal. Very little work has been done to quantify or understanding the effect of such contamination terms from boundary cells for DFEMs in the diffusion limit. We have developed simple test problems to help us quantitatively study the effects of boundary contamination terms. We have used Capsaicin, a transport code developed at LANL, to produce results from standard DFEMs for these test problem.

2. BACKGROUND

A diffusion-limit asymptotic analysis can illuminate connections between the analytic transport equation and the analytic diffusion equation [1,2]. We summarize the main conclusions of this analysis in the simple setting of one energy group and steady state. All of the analysis in this section is derived from previous work. We do not claim to add any new insight to this analysis; however, we attempt to accurately summarize and clarify the boundary layer analysis for general DFEMs.

The steady state transport equation is scaled to be optically thick and diffusive:

$$\vec{\Omega}\bullet\nabla\psi\left(r,\vec{\Omega}\right)+\frac{\sigma\left(\vec{r}\right)}{\varepsilon}\psi\left(\vec{r},\vec{\Omega}\right)=\frac{1}{4\pi}\left(\frac{\sigma\left(\vec{r}\right)}{\varepsilon}-\varepsilon\sigma_a\left(\vec{r}\right)\right)\phi\left(\vec{r}\right)+\varepsilon\frac{Q\left(\vec{r}\right)}{4\pi} \tag{1}$$

We postulate that the solution, $\psi\left(\vec{r}\right)$, to this scaled equation is a power series in ε.

$$\psi\left(\vec{r}\right)=\psi^{(0)}+\varepsilon\psi^{(1)}+\varepsilon^2\psi^{(2)}+\ldots \tag{2}$$

From Eq. (1) and (2), for the analytic transport equation, we find that the leading-order angular flux is isotropic and satisfies a diffusion equation in the interior of the spatial domain.

$$\begin{aligned}&-\nabla\bullet\frac{1}{3\sigma\left(\vec{r}\right)}\nabla\phi^{(0)}\left(\vec{r}\right)+\sigma_a\left(\vec{r}\right)\phi^{(0)}\left(\vec{r}\right)=Q\left(\vec{r}\right)\\&\psi^{(0)}\left(\vec{r},\vec{\Omega}\right)=\frac{1}{4\pi}\phi^{(0)}\left(\vec{r}\right),\ \vec{r}\in\text{interior zones}\end{aligned} \tag{3}$$

Eq. (3) is not a well-posed mathematical problem without appropriate boundary conditions for the leading-order solution. We consider Eq. (3) to be a statement of the leading-order solution's behavior in the interior of the problem. From the diffusion limit asymptotic analysis of the analytic transport equation, the appropriate boundary condition for the leading-order solution is [1]

$$\phi^{(0)}\left(\vec{r}\right) = 2\int_{\vec{n}\bullet\vec{\Omega}<0} d\Omega W\left(\left|\vec{n}\bullet\vec{\Omega}\right|\right)\psi_{inc}\left(\vec{r},\vec{\Omega}\right),\ \vec{r}\in boundary$$
$$W\left(\mu\right) = \frac{\sqrt{3}}{2}\mu \mathrm{H}\left(\mu\right) \approx 0.91\mu + 1.635\mu^2 \approx \mu + \frac{3}{2}\mu^2 \qquad (4)$$

Here $\vec{n}$ is the outward unit normal at the boundary point $\vec{r}$.

One utility of the analysis of the analytic transport equation is to compare it against the results from the same diffusion-limit analysis applied to a discretized version of the transport equation. In order for a transport discretization to accurately represent the physical solution for a optically thick and diffusive problem, its leading-order solution for cells interior to the problem must satisfy a reasonable discretization of the diffusion equation, *and* its discretization of the boundary cells must accurately approximate the boundary conditions given in Eq. (4). For this paper, we assume that the angular discretization applied to the equation is the well-known discrete ordinates (S_N) discretization, and we focus on the results from the family of general, upwind DFEM spatial discretizations.

Demonstrating that appropriately defined DFEMs and CMs lead to valid discretized diffusion equations in the interior has been the goal of several studies, which have utilized both analysis and numerical test problems. [5-12] However, the effect of unresolved boundary layers has received much less attention [5,7], and the conclusions that exist give reason for concern that inexact numerical treatment of the boundary layer may produce significant inaccuracies. To summarize the analysis of the discretized transport equation we follow Adams's asymptotic analysis of DFEMs for the boundary term [5]. Adams shows that the boundary conditions affect the leading-order solution via a discrete Fick's-Law equation that comes from taking the zeroth and first angular moment of the $O(\varepsilon)$ equation. From Adams, we recall Eq. (98), which is derived from the zeroth angular moment of the $O(\varepsilon)$ equation.

$$-\int_V d^3r\vec{\nabla}v_p\left(\vec{r}\right)\bullet\vec{J}^{(1)}\left(\vec{r}\right) + \int_V d^3r v_p\left(\vec{r}\right)\sigma_a\left(\vec{r}\right)\phi^{(0)}\left(\vec{r}\right) = \int_V d^3r v_p\left(\vec{r}\right)q_{ext}\left(\vec{r}\right) \qquad (5)$$

This equation is a balance equation and does not directly include the effect of boundary conditions. We also recall Eq. (106) from Adams, which is the first angular moment of the $O(\varepsilon)$ equation with an erroneous "+" superscript corrected to "–":

$$\frac{1}{3}\sum_{l:\partial V_{kl}\in\partial V}\int_{\partial V_{kl}} d^2r w_{ki}\left(\vec{r}\right)\left[\frac{1}{2}\vec{n}_{kl}\phi^{(0)}\left(\vec{r}_{kl}^{+}\right) + \sum_{m:n_{kl}\bullet\vec{\Omega}_m<0}\Delta_m 3\vec{n}_{kl}\bullet\vec{\Omega}_m\vec{\Omega}_m\psi_{inc}\left(\vec{r}_{kl},\vec{\Omega}_m\right)\right]$$
$$+\frac{1}{3}\sum_{l:\partial V_{kl}\notin\partial V}\int_{\partial V_{kl}} d^2r w_{ki}\left(\vec{r}\right)\vec{n}_{kl}\frac{1}{2}\left[\phi^{(0)}\left(\vec{r}_{kl}^{-}\right)+\phi^{(0)}\left(\vec{r}_{kl}^{+}\right)\right] \qquad (6)$$
$$-\frac{1}{3}\int_{V_k} d^3r\phi^{(0)}\left(\vec{r}\right)\vec{\nabla}w_{ki}\left(\vec{r}\right) + \int_{V_k} d^3r w_{ki}\left(\vec{r}\right)\sigma\left(\vec{r}\right)\vec{J}^{(1)}\left(\vec{r}\right) = 0$$

where

$w \equiv$ FEM weight function

$\Delta \equiv$ quadrature weight

$i \equiv$ FEM weight function index

$k \equiv$ mesh cell index

$l \equiv$ surface index for a cell

$\vec{r}_{kl}^{-} \equiv$ spatial coordinate just inside cell k's surface l

$\vec{r}_{kl}^{+} \equiv$ spatial coordinate just outside cell k's surface l

$\vec{n}_{kl} \equiv$ outward unit normal for cell k's surface l

$\partial V_{kl} \equiv$ Cell k's surface l area (length in 2D)

$dV \equiv$ Problem domain boundary

$V_{kl} \equiv$ Volume (area in 2D) of cell k

Eq. (6) is generalized for boundary cells, and therefore does include the effects of boundary conditions. Essentially, Eqs. (5) and (6) represent a system of two equations with two unknowns: $\vec{J}^{(1)}\left(\vec{r}\right)$ and $\phi^{(0)}$. We can solve Eq. (6) for $\vec{J}^{(1)}\left(\vec{r}\right)$ in terms of $\phi^{(0)}$, and substitute this result into Eq. (5) to produce a discretized diffusion equation satisfied by $\phi^{(0)}$. The divergence theorem replaces the w_{ki}-weighted integral of the gradient with three terms: a volume integral involving ∇w_{ki}, a surface integral for problem-interior surfaces, and a surface integral for problem-boundary surfaces. It is important to note that the "problem" may be a diffusive *region* in a larger problem. We will use this idea in the development of a test problem that approximates a real physical system. Also, a symmetric quadrature set is assumed throughout the analysis and test problem development. Because all boundary conditions are confined in the first line of Eq. (6), we will use these terms for the basis of most of our discussion.

We begin the discussion of the boundary layer analysis by examining the problem-boundary term for one cell surface (Eq. (118) from Adams and the first line in Eq. (6)):

$$DFEM\ boundary\ term = A_{kl}\left[\frac{1}{2}\vec{n}_{kl}\phi_{kli}^{(0)} + \sum_{m:n_{kl}\bullet\vec{\Omega}_m<0} \Delta_m 3\vec{n}_{kl}\bullet\vec{\Omega}_m\vec{\Omega}_m\psi_{inc,kli}\left(\vec{\Omega}_m\right)\right], \qquad (7)$$

where

$$\phi_{kli}^{(0)} \equiv \frac{1}{A_{kl}}\int_{\partial V_{kl}} d^2 r w_{ki}\left(\vec{r}\right)\phi^{(0)}\left(\vec{r}\right)$$
$$A_{kl} \equiv \int_{\partial V_{kl}} d^2 r \qquad , \qquad (8)$$

(For simplicity we have assumed that each cell surface on the problem boundary is planar, which allows the unit normal to move outside the spatial integral.) The analytic analog of this boundary term is developed by multiplying Eq. (4) by the DFEM weight function, w_{ki}, and integrating over the surface. The integral over direction is approximated with a discrete-ordinates quadrature sum, resulting in what Adams calls the *ideal term* (Eq. (117) from Adams).

$$\textit{ideal term} = A_{kl}\vec{n}_{kl}\,2\sum_{\mu_m<0}\Delta_m W\left(\left|\mu_m\right|\right)\psi_{inc,kli}\left(\vec{\Omega}_m\right)\ ,\ \ \mu_m \equiv \vec{n}_{kl}\bullet\vec{\Omega}_m\ . \tag{9}$$

The best DFEMs, even in 1D slab geometry, do not achieve the ideal term shown here. However, the best DFEMs do achieve an excellent approximation to the ideal term, which we refer to as "DFEM-ideal:"

$$\textit{DFEM-ideal term} = A_{kl}\vec{n}_{kl}\,2\sum_{\mu_m<0}\Delta_m\left[\frac{\left|\mu_m\right|}{\rho_{kl}}+\frac{3}{2}\mu_m^2\right]\psi_{inc,kli}\left(\vec{\Omega}_m\right)\ ,\ \ \mu_m \equiv \vec{n}_{kl}\bullet\vec{\Omega}_m \tag{10}$$

This is the ideal term except that the *W* function has been replaced by a quadratic polynomial that is known to be accurate to within a few percent [1]. This *DFEM-ideal* term is the standard to which we will compare the actual DFEM term.

When examining the zeroth moment of the *O*(1) equation in the asymptotic analysis, Adams derived an expression for the leading-order scalar flux on the boundary (Eq. (77) from Adams):

$$\begin{aligned}\phi_{kli}^{(0)} &= 2\sum_{m:n_{kl}\bullet\vec{\Omega}_m<0}\Delta_m\frac{2\vec{n}_{kl}\bullet\vec{\Omega}_m}{\rho_{kl}}\psi_{inc,kli}\left(\vec{\Omega}_m\right),\ \vec{r}_{kl}\in\partial V\\ \rho_{kl} &\equiv \frac{2\sum_{m:n_{kl}\bullet\vec{\Omega}_m<0}\Delta_m\vec{n}_{kl}\bullet\vec{\Omega}_m}{\sum_{m:n_{kl}\bullet\vec{\Omega}_m<0}\Delta_m}\approx 1\end{aligned} \tag{11}$$

Substituting this expression into Eq. (10) results in

$$\textit{DFEM boundary term} = A_{kl}\left[\sum_{m:n_{kl}\bullet\vec{\Omega}_m<0}\Delta_m\left[\vec{n}_{kl}\frac{2\left|\mu_m\right|}{\rho_{kl}}+3\vec{n}_{kl}\bullet\vec{\Omega}_m\vec{\Omega}_m\right]\psi_{inc,kli}\left(\vec{\Omega}_m\right)\right] \tag{12}$$

We note that

$$\begin{aligned}\mu_m &= \vec{n}_{kl}\bullet\vec{\Omega}_m\\ \vec{\Omega}_m &= \mu_m\vec{n}_{kl}+\vec{\omega}_m\end{aligned} \tag{13}$$

Here $\vec{\omega}_m$ is the tangential component of the direction vector $\vec{\Omega}_m$. Substituting these definitions into Eq. (12) results in

$$\textit{DFEM boundary term} = A_{kl}\left[\sum_{m:n_{kl}\bullet\vec{\Omega}_m<0}\Delta_m\left[\vec{n}_{kl}\frac{2\left|\mu_m\right|}{\rho_{kl}}+3\vec{n}_{kl}\mu_m^2+3\mu_m\vec{\omega}_m\right]\psi_{inc,kli}\left(\vec{\Omega}_m\right)\right] \tag{14}$$

We simplify Eq. (14) to contain an ideal component and a contamination component.

$$\begin{aligned}\textit{DFEM boundary term} = A_{kl}\vec{n}_{kl}\,2\sum_{m:n_{kl}\bullet\vec{\Omega}_m<0}\Delta_m\left[\frac{\left|\mu_m\right|}{\rho_{kl}}+\frac{3}{2}\mu_m^2\right]\psi_{inc,kli}\left(\vec{\Omega}_m\right)\\ +A_{kl}\sum_{m:n_{kl}\bullet\vec{\Omega}_m<0}\Delta_m 3\mu_m\vec{\omega}_m\psi_{inc,kli}\left(\vec{\Omega}_m\right)\end{aligned} \tag{15}$$

The first line of Eq. (15) is the ideal term found in Eq. (10). This DFEM-ideal term is dependent on the quadrature order through the ρ_{kl} factor. As ρ_{kl} approaches 1, the DFEM-ideal term better approximations the analytic term in Eq. (9). Table I lists ρ_{kl} values for the standard level symmetric quadrature set.

Table I. ρ_{kl} for the Level Symmetric Quadrature set

S_N Order	ρ_{kl}
2	1.15470054
4	1.04595510
6	1.02648088
8	1.01702734
10	1.01271533
12	1.00974740
14	1.00801134
16	1.00662993
18	1.00572395

The second line of Eq. (15) is the tangential "contamination" term, the boundary term whose quantitative effects we would like to explore with suitable test problems. This contamination term is naturally mitigated in multiple ways. If the tangential component of the incident flux is isotropic and the quadrature set is symmetric, the contamination term is zero. This property is obvious from Eq. (15). The positive values of the tangential angles cancel with the negative values. Furthermore, the contamination term affects the solution through a dot product of the gradient of a weight function and the first-order current, $\vec{J}^{(1)}\left(\vec{r}\right)$, which is easy to see from Eqs. (5) and (6).

It is important to not confuse the contamination term with a Marshak boundary condition. Recall that DFEM solutions have one unknown per vertex in each cell. Larsen and Morel [4] demonstrated that in the thick diffusion limit, for cells on the boundary of the thick region DFEMs will have solutions that are equivalent to a Marshak boundary conditions for unknowns whose vertices are adjacent to the physical boundary, and a different boundary condition value for the other vertices in the cell. This different boundary condition is consistent with the boundary terms we have been defining in Eq. (7). These interior boundary conditions are what define the leading-order boundary conditions for the interior diffusion solution, and are the vertices which may contain the contamination term in the discretized boundary layer.

3. TEST PROBLEM DESCRIPTION

We have shown in Eq. (15) that a DFEM discretization of the boundary cells results in a two-term expression for the discretized solution in the boundary cells. The first term is a good approximation of Eq. (4). The second term is a tangential contamination term that vanishes if the incident intensity has sufficient azimuthal symmetry that the discrete half-range integral in the last term of Eq. (15) equals zero. (For example, 180-degree rotational symmetry in the azimuthal

angle is sufficient to make the term vanish.) Otherwise the contamination term persists. We have developed two test problems that explore the error caused by the boundary layer contamination term.

3.1 Test Problem 1: Rigorously Zero Solution Test Problem

Our first test problem is designed such that the leading order scalar flux goes to zero everywhere in the problem for orthogonal grids except for the boundary zones next to a non-zero incident angular flux Dirichlet boundary condition. To derive these conditions, we simply set the leading order flux in Eq. (10) to zero.

$$DFEM\text{-}ideal\ term = A_{kl}\vec{n}_{kl}\,2\sum_{\mu_m<0}\Delta_m\left[\frac{|\mu_m|}{\rho_{kl}}+\frac{3}{2}\mu_m^2\right]\psi_{inc,kli}\left(\vec{\Omega}_m\right)=0\ ,\ \ \mu_m\equiv\vec{n}_{kl}\bullet\vec{\Omega}_m\,. \tag{16}$$

If we enforce this condition along the *entire* boundary, for a problem that is optically thick and highly scattering, and include no other sources in the problem, than this boundary condition will lead to a leading-order interior solution that is zero for orthogonal grids. The leading-order solution should be zero for orthogonal grids because the boundary layer contamination terms, which affect the first order current, will cancel each other out along the boundary through the dot product of the current and the gradient of the weight functions. However, we will observe some propagation of the contamination term on a non-orthogonal grid because the components of this dot product are not guaranteed to cancel each other in the boundary layer. As a result, this test problem will be useful for observing how far the contamination term can numerically diffuse into the interior solution. To measure this numerical diffusion, we simply plot the deviation of the scalar flux from zero in the problem interior.

For this problem, we define an incident angular flux in terms of a tangential direction only. This incident flux will be the *only* source of particles in the problem. We derive this boundary condition for 2D XY transport, and use standard direction cosine notation.

$$\psi_{inc}\left(\vec{r},\vec{\Omega}_m\right)=a+b\eta_m+d\eta_m^2 \tag{17}$$

We use the definition of the "manufactured" incident angular flux in Eq. (16) to determine coefficients for ψ_{inc} that lead to a value of zero for the leading-order boundary condition to the interior leading-order diffusion discretization.

$$\Phi^{(0)}\left(\vec{r}\right)=A_{kl}\vec{n}_{kl}\,2\sum_{\mu_m<0}\Delta_m\left[\frac{|\mu_m|}{\rho_{kl}}+\frac{3}{2}\mu_m^2\right]\left\{a+b\eta_m+d\eta_m^2\right\}=0 \tag{18}$$

The summation associated with the *b* term is zero because it is odd with respect to η_m. As a result, we can find values of a and d that to satisfy Eq. (16).

$$a=-\left\{\frac{\displaystyle\sum_{\mu_m<0}\Delta_m\left[\frac{|\mu_m|}{\rho_{kl}}+\frac{3}{2}\mu_m^2\right]\eta_m^2}{\displaystyle\sum_{\mu_m<0}\Delta_m\left[\frac{|\mu_m|}{\rho_{kl}}+\frac{3}{2}\mu_m^2\right]}\right\}d \tag{19}$$

This test problem can also be discussed in terms of the analytic ideal boundary term from Eqs. (4) and (9). We express the manufactured solution for ψ_{inc} in a non-discrete form

$$\begin{aligned} \psi_{inc}\left(\vec{r},\vec{\Omega}\right) &= a + b\eta + d\eta^2 \\ \eta &= \left(1-\mu^2\right)^{1/2}\sin\gamma \end{aligned} \tag{20}$$

To define the coefficients of this angular flux such that the leading-order angular flux will be zero, substitute Eq. (20) into Eq. (4), using the approximation for *W*, then set the expression equal to zero. Again, the integral associated with the *b* coefficient will automatically be zero. As a result, we can define *a* and *d* such that leading-order scalar flux is zero:

$$\begin{aligned} \Phi^{(0)}\left(\vec{r}\right) &\approx 2\int_0^{2\pi} d\gamma \int_0^1 d\mu \left(\mu + \frac{3}{2}\mu^2\right)\left(a + d\left(1-\mu^2\right)\cos^2\gamma\right) = 0 \\ 2\pi\left(\frac{1}{2}+\frac{1}{2}\right)a + \pi\left(\frac{1}{2}-\frac{1}{4}+\frac{1}{2}-\frac{3}{10}\right)d &= 0 \\ 2a &= -0.45d \\ a &= -\{0.225\}\,d \end{aligned} \tag{21}$$

We can use the results from Eqs. (19) and (21) to draw some simple conclusions about errors due to quadrature order. The coefficients in front of d should be equivalent. Table II contains the value of this coefficient for different orders of the level symmetric quadrature set. A sufficiently accurate quadrature set will match the value of 0.225, and as the quadrature order increases, this coefficient should approach this value.

Table II. Test Problem 1 Coefficient for the Level Symmetric Quadrature set

S_N Order	Coefficient
2	0.33333333
4	0.23180627
6	0.22865891
8	0.22725946
10	0.22666166
12	0.22625939
14	0.22602887
16	0.22584719
18	0.22572917

It is important to note that, in 3D, the definition of the test problem given in Eq. (19) and Eq. (21) is invariant for ξ and η. The coefficients resulting from the integration are the same in both cases.

3.2. Test Problem 2: Error Magnitude for the Boundary Layer Contamination Term

We have developed the second test problem for two reasons. First, Test Problem 1 only develops a shape for the error due to the contamination term on non-orthogonal grids. The second test problem will better quantify the magnitude of this error, and will be applicable to studying the contamination term on orthogonal grids. Second, we want to connect the effect of the contamination term to reality, so we have developed a thick, diffusive test problem that is connected to a simplified, but reasonable physics simulation.

The basic manufactured solution for Test Problem 2 is a one-term expression for ψ_{inc}, where ψ_{inc} is defined with three, slightly different dependencies on η. We summarize these definitions in Table III, and note that this discussion assumes we are interested in the leading-order solution in the thick, diffusive limit. The Ideal interior solution is the solution for the leading-order flux given a DFEM-ideal term (Eq. (10)) for the interior boundary condition.

Table III. Summary of ψ_{inc} cases for second boundary layer manufactured solution

Case	ψ_{inc}	DFEM boundary term	Contamination term	Ideal interior solution	Actual interior solution
1	$a\,,\forall\,\eta_m$	**Non-Zero**	**Zero**	**Non-zero**	**Ideal**
2	$\begin{cases} a\,,\eta_m > 0 \\ -a\,,\eta_m < 0 \end{cases}$	**Zero**	$\propto 2a$	**Zero**	**Ideal + Contamination**
3	$\begin{cases} 2a\,,\eta_m > 0 \\ 0\,,\eta_m < 0 \end{cases}$	**Non-Zero**	$\propto 2a$	**Non-zero, = Case 1**	**Ideal + Contamination**

Case 3 is a numerical test problem that describes the types of boundary layers that exist in a simplified physics simulation. This simplified physics problem, shown in Figure 1, consists of a thin region next to a thick region with an incident angular flux on the minimum y face of the problem. At the boundary between the thin and thick region, this incident flux will cause the boundary layer effect described in Case 3. The spatial definition of Case 3, with is prescribed boundary conditions, can also be found in Figure 1.

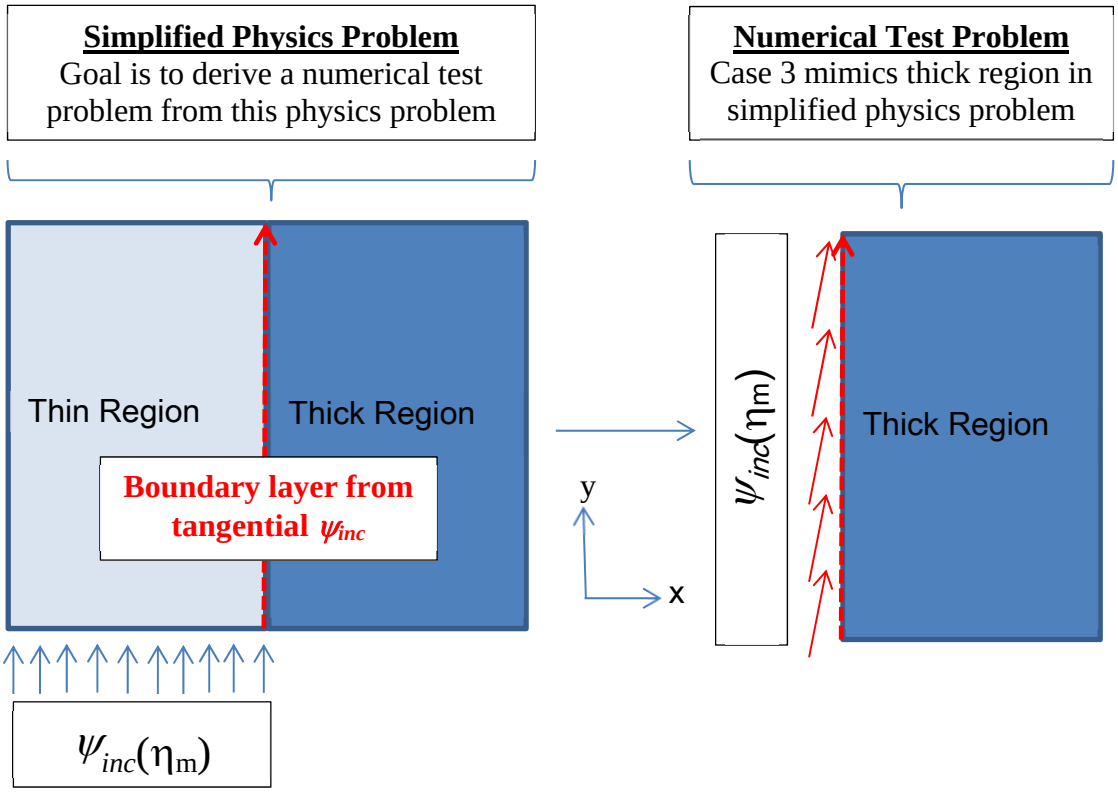

Figure 1. Simplified Physics Problem that leads to Case 3 of Test Problem 2

Because the ideal interior solution for Case 3 and Case 1 are equivalent, but the actual interior solution of Case 3 is the ideal solution with the contamination effect, we can use the difference between Case 3 and Case 1's actual solutions to find the error due to contamination. Furthermore, we observe that Case 1 + Case 2 will yield Case 3 due to superposition. As a result, the solution of Case 2 is the error due to contamination in Case 3, and Case 1 provides a reference solution to understand the magnitude of that error. We only need solutions to Case 1 and Case 2 to quantify the error due to the boundary layer contamination term for an approximate physical problem.

For this test problem, we recommend that the non-zero incident angular flux only be specified for a few cells above and a fell cells below the geometric center point of the problem boundary. This spatially discontinuous boundary condition will prevent the cancellation of contamination terms through the dot product operation. We should observe error in both orthogonal and non-orthogonal grid cases.

3.3. Summary of Test Problems

We have developed two test problems to explore the contamination term that arises in the boundary layer analysis of DFEMs. The first test problem uses an incident angular flux to produce an interior leading-order solution that is rigorously zero if the DFEM boundary layer

term is not influenced by the contamination term. We apply this boundary condition at every point along the boundary. As a result, we expect a DFEM to produce this zero leading-order scalar flux on an orthogonal grid when the material properties cause the problem to be sufficiently thick and diffusive. We can use this problem to explore errors due to grid distortion as well as unresolved quadrature sets. The limitation of this test problem is that it will show the shape of the error from the contamination term, but it does not allow us to quantify the magnitude of the error compared with an exact solution.

The second family of test problems is more powerful because it allows us to find a magnitude (Case 1) and shape (Case 2) of the error due to the contamination term. This test problem also has a physically meaningful interpretation (Case 3). We use the concept of superposition to separate out the magnitude and shape of the error.

4. RESULTS

We ran these two test problems using Capsaicin, a radiation transport research code being developed at Los Alamos National Laboratory [13]. These problems were run using the 2D XY Fully Lumped Bi-linear Discontinuous Finite Element spatial discretization, which has been shown to recover the diffusion limit both analytically and numerically [5].

4.1 Results for Test Problem 1

We first ran this test problem with decreasing values of ε to show that as the problem becomes sufficiently thick and diffusive ($\varepsilon \to 0$), it converges. This ε-scaling procedure was introduced by Warsa et al. [14] as a mechanism to numerically determine if an S_N discretization will succeed in the thick diffusion limit. Parameters for the ε–scaling of Test Problem 1, are found in Table III, where the total and absorption cross sections are multiplied by 2^n ($1/\varepsilon$) and $1/2^n$ (ε), respectively.

Table III. Test Problem 1 Parameters

Parameter	Value
a (coefficient for ψ)	-14.45422016
b(coefficient for ψ)	0.0
d (coefficient for ψ)	64.0
Total Cross Section	$1*2^n$
Absorption Cross Section	$0.5/2^n$
Quadrature Set	S16, Level Symmetric
Boundary conditions	Left: Incident Flux Top: Reflecting Bottom: Reflecting Right: vacuum
Tolerance	1E-12, relative error
Acceleration	DSA preconditioned GMRES

The results for the ε-scaling of Test Problem 1 are found in Figure 2 (orthogonal grid) and Figure 3 (non-orthogonal, randomized grid). This problem was run with a 64x64 mesh. The non-orthogonal grid was created by randomizing the vertices of the orthogonal grid. We plot the cell-averaged scalar flux for interior cells at a cut line through the cells just above y=2 for values of n=10 through n=20.

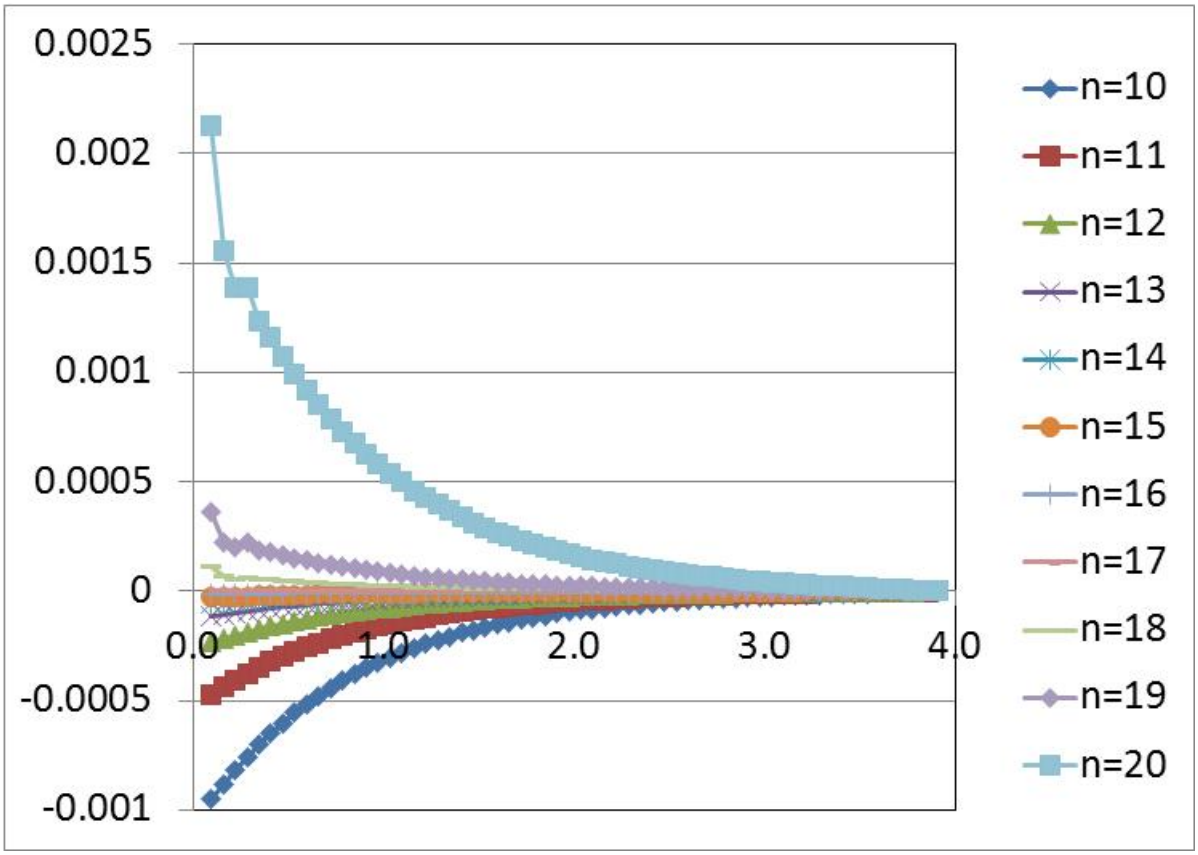

Figure 2. Results of ε-scaling for Test Problem 1 on an orthogonal grid

For the orthogonal grid solution in Figure 2, the solution appears to be converging up to n=17, then becomes unstable for n>17 (very large ε). However, we believe that this behavior is not a lack of convergence, but a demonstration of round-off error accumulation due to lack of machine precision. Warsa, et.al. [14] noted this same behavior, and, coincidentally, found they needed to add precision at n=18. As a result, we will use a value of n=17 in the remainder of our results. Figure 3 demonstrates that the non-orthogonal grid case is converging with respect to ε, and it is converging to a non-zero solution. We believe that we do not have the same problem with machine round-off for the non-orthogonal case because the solution is non-zero, and round-off errors have a much smaller effect on non-zero solutions than zero solutions. This non-zero solution for the non-orthogonal grid case is the effect of the contamination term for interior cells. In Figure 4, we show the 2D cell-averaged scalar flux for both the orthogonal and non-orthogonal grid. The contours in these plots are on a log scale and represent the absolute value of the scalar flux. It is important to note that Test Problem 1 demonstrates that the contamination term is pronounced in the non-orthogonal grid case, but we need test problem 2 to determine its

potential magnitude. It is also important to note that, in Figure 4, we observe a very small amount of contamination for the orthogonal grid case.

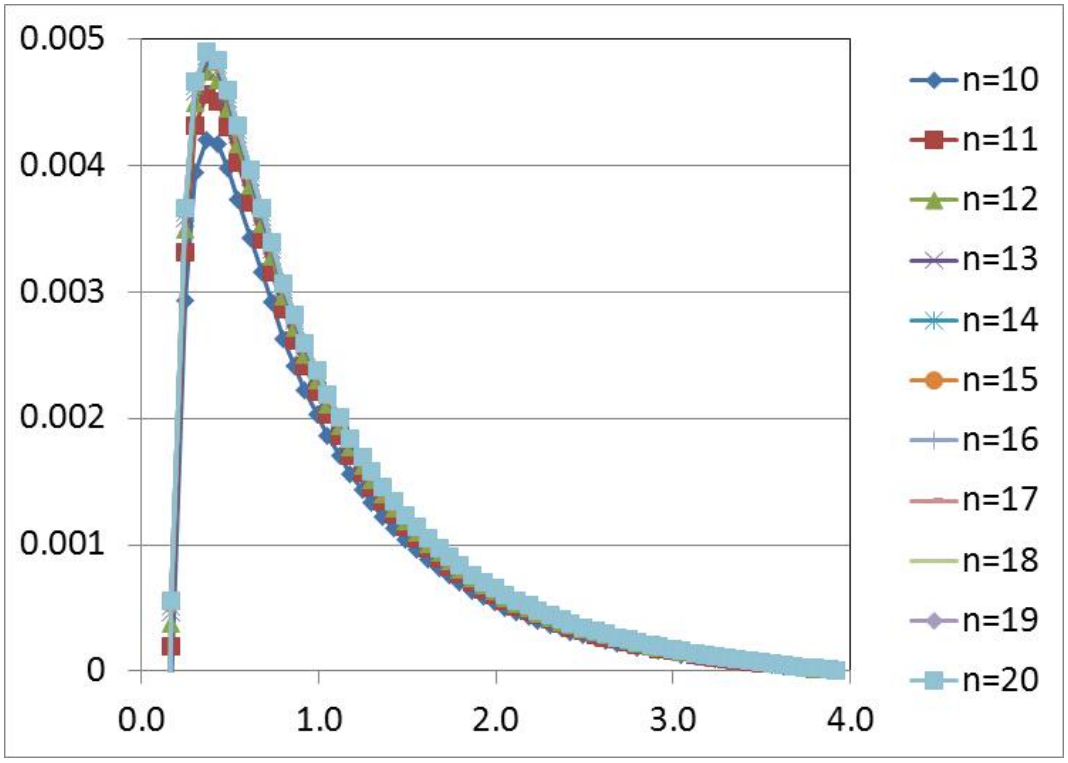

Figure 3. Results of ε-scaling for Test Problem 1 on an orthogonal grid

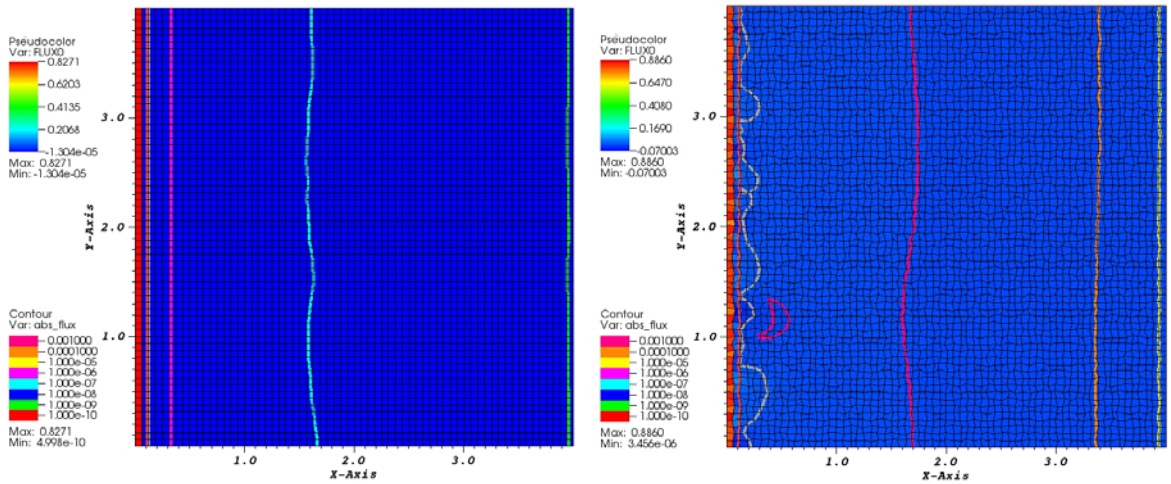

Figure 4. Test Problem 1 Cell-Averaged Scalar flux for Orthogonal and Non-orthogonal Grids

4.2 Results for Test Problem 2

The second test problem only requires a single coefficient value. We use a =1.0, apply the boundary condition on the minimum x face of the problem domain for two zones above and below the y-midpoint, and use the same physical constants from Table III. We run this problem on the orthogonal and non-orthogonal grids used in Test Problem 1, and shown in Figure 4.

For orthogonal grids, the result for Case 1 and Case 2 is show in Figure 5. The pseudocolor plots of the flux are on linear scale, and the contour plots are on a log scale. It is easy to see that the error is largest near the boundary and rapidly decreases inside the problem interior. It is also interesting to note that the error is the negative mirror image at the y-midplane in the problem. This behavior is due, again to the propagation of the contamination term via the current through

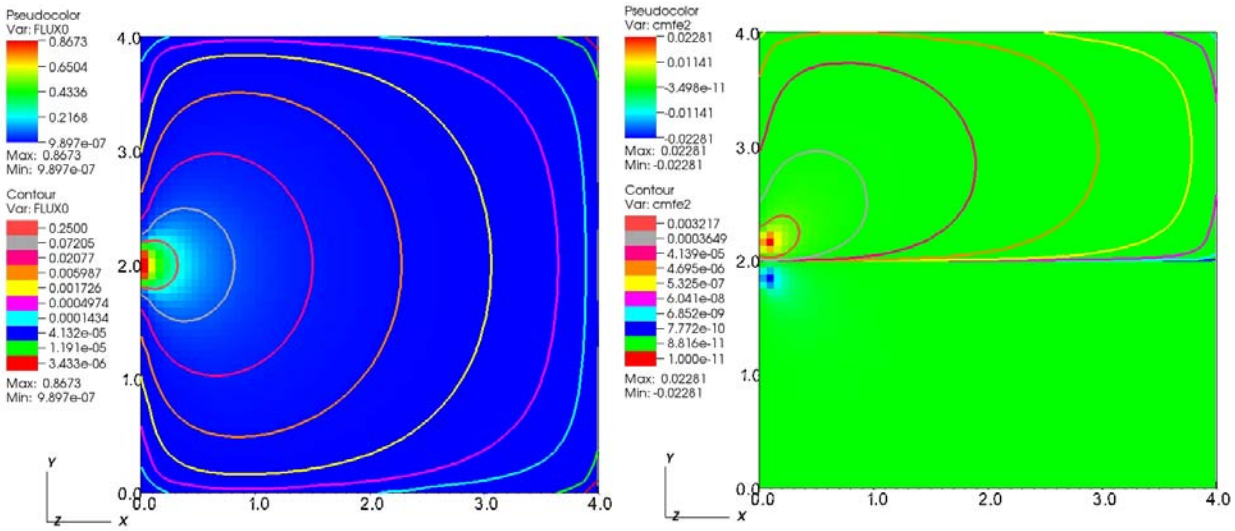

Figure 5. Results for Test Problem 2 on an Orthogonal grid; Case 1: Solution Magnitude (left); Case 2: Solution Error Magnitude (right)

cell edges.

Because we know the solution magnitude and the error due to the contamination term, we also plot a relative error, which is defined as

$$E = \frac{|Error|}{Magnitude} = \frac{|\phi|_{Case\,2}}{\phi_{Case\,1}} \tag{22}$$

The relative error for the orthogonal grid case is found in Figure 6. It is easy to see that the relative error, which is the error in the simulation due to the contamination term, is reasonable small, and quickly decreases away from the boundary. This result is important because we have demonstrated that, although a contamination term exists, we have proof that it is a small source of error in the overall solution.

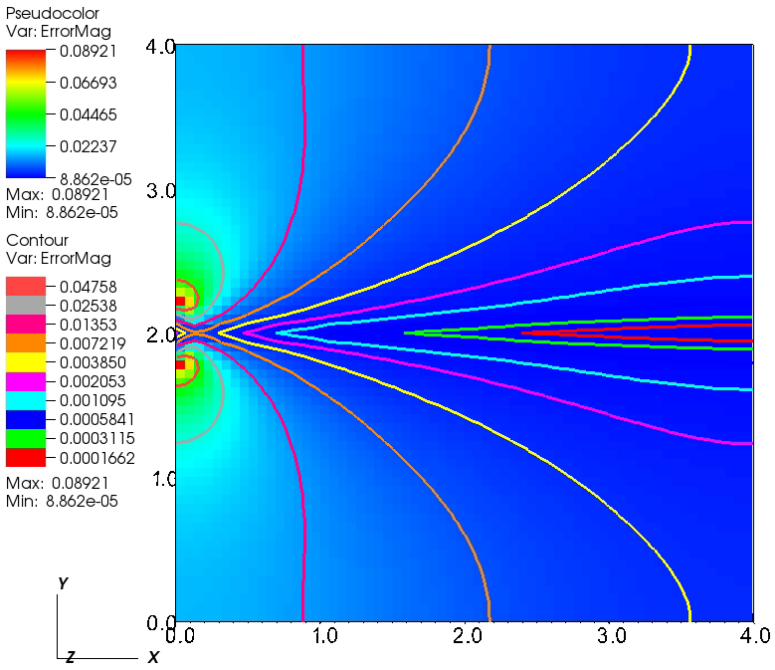

Figure 6. Relative Error for Test Problem 2 on an Orthogonal Grid

We replicate the plots in Figure 5 and Figure 6 for non-orthogonal grids. These results are shown in Figure 7 and Figure 8. The grid distortion changes the shape of the contour plots. The relative error is no longer symmetric and it propagates into the problem interior significantly farther than the orthogonal grid case. Also, the error is non-trivially larger on the non-orthogonal grids.

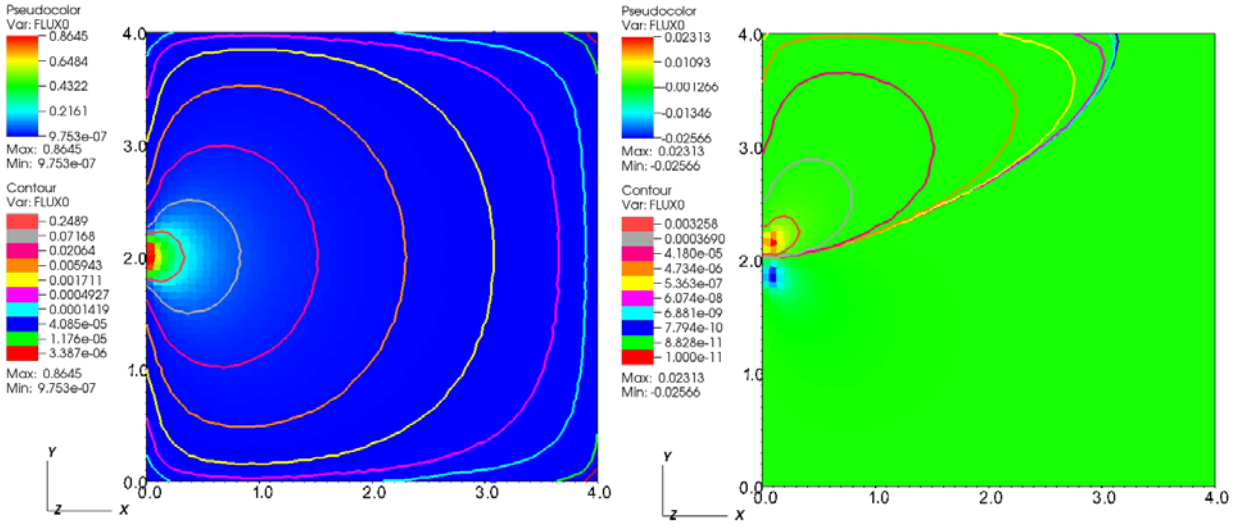

Figure 7. Results for Test Problem 2 on a Non-orthogonal grid; Case 1: Solution Magnitude (left); Case 2: Solution Error Magnitude (right)

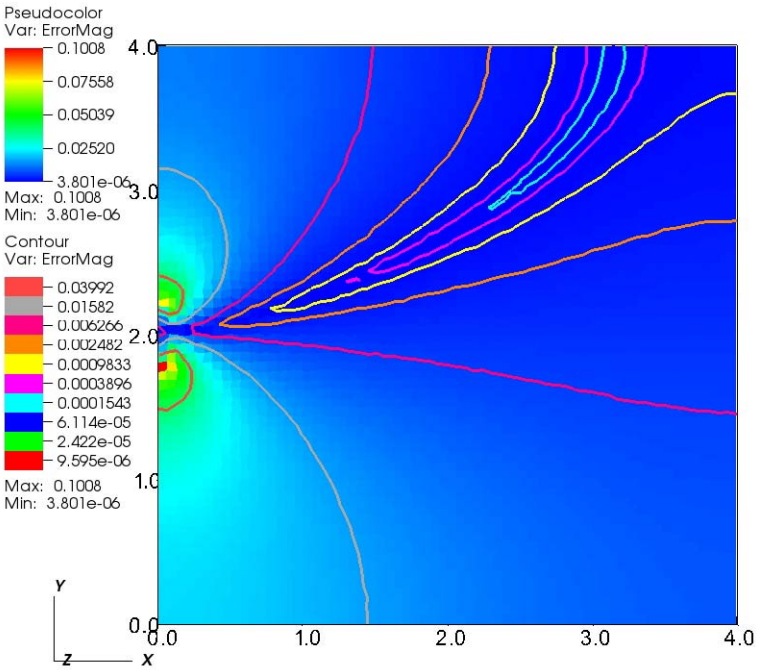

Figure 8. Relative Error for Test Problem 2 on a Non-orthogonal Grid

5. CONCLUSIONS

We have developed boundary layer test problems in the thick diffusion limit to test the effect of the contamination terms that arise in the boundary layer asymptotic thick diffusion limit analysis for both DFEMs and CMs. The first test problem is designed to produce numerically correct behavior for orthogonal grids i.e. the contamination terms are cancelled out due to the regularity of the grid and the applied boundary condition. This first test problem is useful for code verification as well as examining the contamination term effect for non-orthogonal grids. We applied Warsa's ε-scaling methodology to this problem and found that the orthogonal grid case did not converge. We attribute this lack of convergence to machine precision issues, and note that round-off errors will be exacerbated because the solution is converging to zero.

The second test problem is designed to be an approximation of a simplified physics problem. This test problem allows us to solve for a solution magnitude and solution error due to the contamination term. We use these parameters to define a relative error that is useful for understanding the overall effect the contamination term can have in a real simulation.

We have applied these test problems to the fully lumped BLD method using the LANL's Capsaicin code. Both test problems have shown that the contamination terms do propagate into the solution, and that the errors are markedly worse for non-orthogonal grids. We were also able to numerically determine the relative error of this effect using Test Problem 2.

The utility of these test problems to other methods and geometries has not yet been fully explored. We have many suggestions for future work.

- Explore the effect of round-off errors for Test Problem 1
- Examine the CM boundary layer analysis and apply these test problems to CMs in order to compare the accuracy of DFEMs and CMs
- Apply these test problems to a variety of lumping schemes in the general DFEM framework.
- Apply these test problems in 3D Cartesian, and 2D RZ geometries

ACKNOWLEDGMENTS

This work performed under the auspices of the U.S. Department of Energy by Lawrence Livermore National Laboratory under Contract DE-AC52-07NA27344. This information has been authored by employees of the Los Alamos National Security, LLC (LANS) operator of Los Alamos National Laboratory under contract No DE-AC52-06NA25396 with the U.S. Department of Energy.

REFERENCES

1. F. Malgavi and G. C. Pomraning, "Initial and Boundary Conditions for Diffusive Linear Transport Problems," *J. Math. Phys.*, **32**, 805-820 (1990).
2. E. W. Larsen, G. C. Pomraning, and V. C. Badham, "Asymptotic Analysis of Radiative Transfer Problems," *J. Quant. Spectrosc. Radiat. Trans.*, **29**, 285-310 (1983).
3. E. W. Larsen, J. E. Morel, and W. F. Miller, Jr., "Asymptotic Solutions of Numerical Transport Problems in Optically Thick, Diffusive Regimes I," *J. Comput. Phys.*, **69**, 283 (1987).
4. E. W. Larsen and J. E. Morel, "Asymptotic Solutions of Numerical Transport Problems in Optically Thick, Diffusive Regimes II," *J. Comput. Phys.*, **83**, 212 (1989).
5. M. L. Adams, "Discontinuous Finite Element Transport Solutions in Thick Diffusive Problems," *Nucl. Sci. and Eng.* **137**, 298-333 (2001).
6. J. L. Guermond and G. Kanschat, "Asymptotic Analysis of Upwind Discontinous Galerkin Approximation of the Radiative Transport Equation in the Diffusion Limit," *SIAM J. Numer. Anal.*, **48**, 53-78 (2010).
7. M. L. Adams, T. A. Wareing, and W. F. Walters, "Characteristics Methods in Thick Diffusive Problems," *Nucl. Sci. and Eng.* **130**, 18-46 (1998).
8. T. M. Pandya, "Long-Characteristics Methods with Piecewise Linear Sources in Space and Time for Transport on Unstructured Grids," Doctoral Dissertation, Texas A&M University (2012).
9. T. S. Bailey, "The Piecewise Linear Discontinuous Finite Element Method Applied to the RZ and XYZ Transport Equations," Doctoral Dissertation, Texas A&M University (2008).
10. G. G. Davidson and T. S. Palmer, "Finite Element Transport Using Wachspress Rational Basis Functions on Quadrilaterals in Diffusive Regions," *Nucl. Sci. and Eng.* **159**, 242-255 (2008).
11. J. E. Morel and J. S. Warsa, "An S_n Spatial Discretization Scheme for Tetrahedral Meshes," *Nucl. Sci. and Eng.* **151**, 157-166 (2005).

12. J. E. Morel, A. Gonzalez-Aller, and J. S. Warsa, “A Lumped Linear-Discontinuous Spatial Discretization Scheme for Triangular-Mesh S_n Calculations in r-z Geometry,” *Nucl. Sci. and Eng.* **155**, 168-178 (2007).
13. K. Thompson, K. Budge, J. Chang, and J. Warsa, “Release of Capsaicin-2_4_0,” LA-UR-05-2256, Los Alamos National Laboratory (2005).
14. J. S. Warsa, J. D. Densmore, and J. E. Morel, “Manufactured Solutions in the Thick Diffusion Limit,” *Nucl. Sci. and Eng.* **166**, 36-47 (2010).